More Efficient Energy Management for Networked Hybrid AC/DC Microgrids With Multivariable Nonlinear Conversion Losses

Zhao, Tianyang; Liu, Xiong; Wang, Peng; Blaabjerg, Frede

Published in:
I E E E Systems Journal

DOI (link to publication from Publisher):
10.1109/JSYST.2022.3215594

Publication date:
2023

Document Version
Accepted author manuscript, peer reviewed version

More Efficient Energy Management for Networked Hybrid AC/DC Microgrids with Multivariable Nonlinear Conversion Losses

Tianyang Zhao, *Senior Member, IEEE,* Xiong Liu, *Senior Member, IEEE,* Peng Wang, *Fellow, IEEE* and Frede Blaabjerg, *Fellow, IEEE*

***Abstract*—Accurate conversion loss models are the keys to guarantee the more efficient operation of networked hybrid AC/DC microgrids (N-AC/DC-MGs). A two-stage stochastic unit commitment (UC) problem is proposed to improve the operational efficiency of N-AC/DC-MGs under uncertain renewable energy generation output and loads. The nonlinear power losses of AC/DC converters and DC/DC converters under different operating modes are formulated as novel multivariate nonlinear functions of both power and voltage. These functions are approximated by linear surrogate models and adopted by the dynamic optimal power flow (OPF), where the voltage and power of the converters can be optimized considering the physical laws among voltages of converters. Embedding the dynamic OPF problem as mixed-integer recourse, a two-stage stochastic programming problem is formulated for the day-ahead operation of N-AC/DC-MGs. To reduce the computational cost, a finite iteration convergent Benders decomposition algorithm is proposed to solve the UC problem. Case studies are performed on hybrid AC/DC MGs and N-AC/DC-MGs. Simulation results reveal that using more accurate conversion loss models, the output commands, especially the DC bus voltage, from the energy management systems will lead to more efficient system operation and thus save energy.**

***Index Terms*—Hybrid AC/DC microgrids, conversion losses, linear surrogate models, two-stage stochastic programming with mixed-integer recourse.**

NOMENCLATURE

A. Indexes and sets

$g \in \mathcal{G}$	Generator set
$d \in \mathcal{D}$	Demand set
$c \in \mathcal{C}$	Bi-directional AC/DC converter set
$v \in \mathcal{V}$	Bi-directional DC/DC converter set
$t \in \mathcal{T}$	Scheduling time period set

B. Parameters

$S_{\mathrm{C},i}$	Rated power for converter i
$h_{\mathrm{E,on},c}, k_{\mathrm{E,on},c}$	Switch-on loss parameters of converter c
$h_{\mathrm{E,off},c}, k_{\mathrm{E,off},c}$	Switch-off loss parameters of converter c
$h_{\mathrm{D},c}, k_{\mathrm{D},c}$	Diode loss parameters of converter c
$f_{\mathrm{S},c}, f_{\mathrm{S},v}$	Switching frequency of converter [Hz]
η_c, η_v	Inductor loss percentage of converter c and v
$R_{\mathrm{T},c}, R_{\mathrm{T},v}$	Conduction resistance of IGBT [Ω]
$R_{\mathrm{D},c}, R_{\mathrm{D},v}$	Conduction resistance of diode [Ω]
$V_{\mathrm{D},c}, V_{\mathrm{D},v}$	Diode forward voltage drop [V]
$V_{\mathrm{T},c}, V_{\mathrm{T},v}$	IGBT forward voltage drop [V]
m_c	Modulation index
$h_{\mathrm{E,on},v}, k_{\mathrm{E,on},v}$	Switching on loss parameters
$h_{\mathrm{E,off},v}, k_{\mathrm{E,off},v}$	Switching off loss parameters
$\bar{V}_c$	Rated DC side voltage of converter c [V]
V^{AC}	Utility grid voltage magnitude [V]
$p_{\mathrm{AC},d}, q_{\mathrm{AC},d}$	Active and reactive power of AC load d
$p_{\mathrm{DC},d}$	DC load d
D_v	Duty cycle
$c_{\mathrm{U},g}, c_{\mathrm{D},g}$	Start-up and shut-down cost of DGs[$]
$V_{l,v}$	Lower side voltage magnitude of DC/DC converters v [V]
R_g	Ramp limitation of generator g [kW/h]
$\bar{P}_{\mathrm{UG},i}$	Maximum power exchange between MG i and the utility grid [kW]
$\underline{E}_{\mathrm{ESS},i}, \bar{E}_{\mathrm{ESS},i}$	Minimum and maximum energy status of ESS i [kWh]
$\underline{P}_g, \bar{P}_g$	Minimum and maximum power output of DG g [kW]
R_{jk}	Resistance of line jk [Ω]

C. Variables

$p_{\mathrm{L},c}, p_{\mathrm{L},v}$	Power losses of converter c,v [kW]
I_c	Root mean square of phase current [A]
$p^t_{\mathrm{UG},i}, q^t_{\mathrm{UG},i}$	Active and reactive power of utility grid
p_g, q_g	Active and reactive power of DG g [A]
$I_{\mathrm{L},v}$	Average current on inductor v [A]
$p_c^{\mathrm{rec}}, q_c^{\mathrm{rec}}$	Active and reactive power of converter c from AC to DC bus [kW, kVar]
p_c^{inv}	Active power of converter c from DC bus to AC bus [kW]
$p_v^{\mathrm{ch}}, p_v^{\mathrm{dc}}$	Active power of converter v
α^t_g, β^t_g	Start-up and shut-down command of generator g
u^t_g	Binary variable, 1 if generator g is online,0 otherwise
p^t_g	Power output of generator g [kW]

This work was supported in part by Guangdong Basic and Applied Basic Research Foundation under Grant 2021A1515110583, in part by the State Key Laboratory of Alternate Electrical Power System with Renewable Energy Sources under Grant LAPS21002. (Corresponding author: *Xiong Liu*)

T. Zhao and X. Liu are with the Energy Electricity Research Center, Jinan University, Guangdong province, China (e-mail: matrixrigs@gmail.com, liushawn123@ieee.org).

P. Wang is with School of Electrical and Electronic Engineering, Nanyang Technological University, Singapore (e-mail: epwang@ntu.edu.sg).

F. Blaabjerg is with the Department of Energy Technology, Aalborg University, DK-9220 Aalborg, Denmark (e-mail: fbl@energy.aau.dk).

$i_{\mathrm{L},v,\min}, i_{\mathrm{L},v,\max}$	Minimum and maximum current [A]
$V_{l,v}$	Inductor voltage of DC/DC converter v [V]
α_{ij}	Continuous variable within [0,1]
h_{ij}^u, h_{ij}^l	Binary variables
$p_{\mathrm{L},c}^{\mathrm{rec},t}, p_{\mathrm{L},c}^{\mathrm{inv},t}$	Conversion losses in the rectification and inversion mode [kW]
$p_{\mathrm{L},c}^{\mathrm{ch},t}, p_{\mathrm{L},c}^{\mathrm{dc},t}$	Conversion losses during the charging and discharging of batteries [kW]
$e_{\mathrm{ESS},i}^t$	Energy stored in the ESSs by the end of time t
$p_{\mathrm{ESS},i}^{\mathrm{ch},t}, p_{\mathrm{ESS},i}^{\mathrm{dc},t}$	Charging and discharging rate of ESSs [kW]
$I_{\mathrm{ESS},i}^{\mathrm{ch},t}, I_{\mathrm{ESS},i}^{\mathrm{dc},t}$	Binary variables, 1 if charging/discharging, 0 otherwise.
$I_{\mathrm{C},i}^{\mathrm{rec},t}, I_{\mathrm{C},i}^{\mathrm{inv},t}$	Binary variables, 1 if rectifying or inverting, 0 otherwise.
$p_{\mathrm{MG},i}^t$	Power exchange between MG i and DC network [kW]
p_{jk}^t	Active power on line jk [kW]

I. Introduction

NETWORKED hybrid AC/DC microgrids (N-AC/DC-MGs) have been recognized as an efficient platform to accelerate the decarbonization transition of power systems [1], [2]. With the maturity of power electronic techniques, the generators, loads, storage systems, and microgrids (MGs) [3] are being integrated into N-AC/DC-MGs via converters. The conversion losses are fundamental factors to be taken care of by the energy management system (EMS), while it is challenged by the multivariable nonlinear relation between power losses, power, current, and voltage [4]. Using more accurate conversion loss models, the output commands from the EMS will lead to more efficient system operation and thus save energy. Under uncertain environments, e.g., renewable energy output and loads, this multivariable nature of power losses might further degenerate the optima derived under classical lossless or linear lossless models [5], [6]. A novel energy management strategy is required to improve the operational efficiency of N-AC/DC-MGs under multivariable conversion losses and uncertainties.

An MG is a group of interconnected loads and distributed energy resources(DERs) within clearly defined electrical boundaries that acts as a single controllable entity concerning the grid, with grid-connected and islanded operation mode [7], including AC, DC, and hybrid AC/DC variations [8]. These MGs can be interconnected by AC networks [9], DC networks [2] or hybrid AC/DC networks [3] formulating the networked MGs (NMGs) [1], [10], increasing the reliability, efficiency, and resiliency. The efficiency management of NMGs has been addressed from generation, demand, storage [11], and network perspectives reducing the power losses [5] and total operational cost [9], [12], e.g., fuel cost.

Conversion is the core functionality of networks within NMGs, using bi-directional AC/DC and DC/DC converters [8]. The conversion losses can be modeled in different approaches, including lossless [11], fixed conversion efficiency [2], current dependent models [5], [13]–[16], power dependent models [17], [18] and voltage/current dependent models [4]. The relation between current and power losses has been widely depicted by a quadratic function for high and medium voltage converters [15], [16], [19], [20]. In the proportional models, the conversion losses are captured by linear functions with fixed efficiency [2], [14], [21]. Conduction and switching losses are two main components of the conversion losses [4]. Considering the impacts of transmission power ratio on conversion efficiency, the conversion losses of AC/DC converters are formulated as quadratic functions [13]. Further accounting for the impacts of voltage, current, and switching frequency on losses, a multivariable nonlinear conversion loss model is proposed for AC/DC converters in [4]. The nonlinear models have been proposed and adopted for AC/DC converters, while the nonlinear nature of DC/DC converter losses has not been explored yet, especially to optimization of the voltage magnitude.

With given conversion loss models, numerous deterministic energy management methods have been proposed to manage the generation, demand, and storage resources within NMGs. These methods are generally formulated as optimization problems, e.g., optimal power flow (OPF) and unit commitment (UC) problems with linear or nonlinear conversion loss models. The linear loss models can be seamlessly integrated into the classical energy management problems, inducing the convex [22] and mixed-integer programming(MIP) problems [23]. The nonlinear loss models lead to nonlinear non-convex optimization problems [13], [22]–[24], which are computational expensive. The piece-wise linear functions have been extensively adopted to approximate the power losses as univariate functions, e.g., current [22], power [13], [17], etc. When the power loss functions are non-convex, binary variables are introduced to reduce the approximation error of piece-wise linear functions [6] and result in MIP problems [25]. These problems can be used to reduce the total cost [6] and power losses [5], under given operating conditions. For NMGs, the relation among voltages of converters is governed by the physical laws of interconnected power networks, e.g., KCL and KVL. They introduces additional constraints among the voltages of converters within NMGs when optimizing the voltages to improve efficiency, which has not been considered in the previous research workes [1], [26].

Inheriting from the deterministic energy management problems, the stochastic [27], robust [2], [28] and distributionally robust [9], [21] optimization problems have been used to manage uncertainties within NMGs, e.g., renewable energy output, loads, and failures. These problems can be further integrated into single-stage [27], two-stage [21] and multi-stage [29] energy management schemes. The conversion losses are omitted for the single-stage stochastic OPF problem in [27]. If the decisions are adjusted after the realization of uncertainties, the two-stage energy management schemes can be adopted. Two-stage stochastic UC problems are proposed for hybrid AC/DC MGs, where the conversion losses are omitted [11] or treated as univariate nonlinear functions [12]. A proportional conversion loss model is adopted by the robust OPF problems [2] and distributionally robust UC problems [21] of N-AC/DC-

MGs. When the decisions can be adjusted more than once, the multi-stage stochastic optimization problems are proposed in [29]. The two-stage optimization, especially the UC problems, has been recognized as a powerful tool to improve the operational efficiency in the day-ahead operation [30].

The two-stage stochastic UC problems can be treated as two-stage stochastic programming problems with continuous recourse [31] or mixed-integer recourse [32], [33]. Using sample average, scenario tree [9], [24], point estimation [11] approximation, this two-stage optimization problem can be reformulated as a large scale MIP problem [12]. It can be solved by either centralized or decomposition algorithms. To reduce the computational cost with a large scale of scenarios, the column generation, row generation, e.g., Benders decomposition, and column & constraint generation [9], [21] decomposition algorithms can be used for the two-stage optimization with continuous recourse. Due to the missing strong optimal conditions of MIP problems, the linear cuts generation methods [34] can be adopted to approximate the mixed-integer recourse.

For low voltage applications in N-AC/DC-MGs, the half-bridge DC/DC converters are widely deployed. This type of DC/DC converter has the buck, boost, and buck-boost operating modes. The switching losses under these operating modes are affected by the voltage directly. To manage the nonlinear conversion losses depending on both voltage and power, a novel multivariable conversion loss model is derived for bi-directional DC/DC converters, where the voltage magnitude can be optimized. The conversion losses models are further incorporated into the energy management problems, where these voltage magnitudes of converters are governed by the physical law on DC networks. The AC/DC and DC/DC conversion loss models are approximated by linear surrogate models and lead to a two-stage stochastic programming problem with mixed-integer recourse. This problem is further solved by an improved Benders decomposition algorithm with the finite iteration convergence guarantee. The main contributions of this work are summarized as follows:

i A novel multivariable power losses model is derived for bi-directional DC/DC converters, including switching losses and conduction losses, w.r.t power, and voltage magnitude.

ii The power losses models are approximated by linear surrogate models as multivariable linear functions, where the voltage magnitude can be optimized to reduce the power losses within hybrid AC/DC MGs.

iii A day-ahead energy management of N-AC/DC-MGs is formulated as a two-stage stochastic UC model with mixed-integer conic recourse, where physical laws among voltage magnitudes of converters are captured.

II. Efficiency Management of Networked Hybrid AC/DC Microgrids

The N-AC/DC-MG is a cluster of hybrid AC/DC MGs $\mathcal{M}$, interconnected by a DC network $\mathcal{G} := \{\mathcal{N}, \mathcal{E}\}$, as shown in Fig. 1 [2]. $\mathcal{N}$ is a set of DC buses, where the set of MGs $\mathcal{M}$ are integrated to. $\mathcal{E}$ is the set of DC lines, interlinking MGs. It is assumed that only one MG is interconnected to the utility grid (UG), while the rest of MGs are connecting to this MG using DC network, e.g., MG i is connecting to the UG, and the rest of MGs connect to MG i using a DC network in Fig. 1 [2]. The resistance of each line $(i, j) \in \mathcal{E}$ is depicted as the weight of arc (i, j) as R_{ij}. The topology of $\mathcal{G}$ can be a tree or mesh grid.

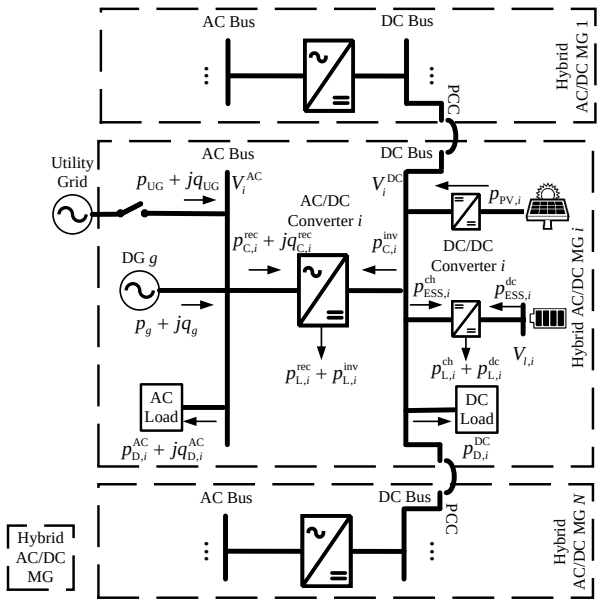

Fig. 1. Single line diagram of networked hybrid AC/DC MGs.

As shown in Fig. 1, within MG i, there exist one AC bus and one DC bus, and the terminal voltage magnitudes are depicted by V_i^{AC} and V_i^{DC}, respectively. The diesel generators (DGs) $g \in \mathcal{G}_i$, UG, and AC loads are integrated into the AC buses. The renewable energy sources, e.g., photovoltaic (PV) generator, energy storage systems (ESSs), and DC loads are integrated into the DC bus, where the ESSs are integrated via bi-directional DC/DC converters $v \in \mathcal{V}$. The AC bus and DC bus are connected by the bi-directional AC/DC converters $c \in \mathcal{C}_i$.

In this work, efficiency management is implemented in the day-ahead operation of energy management systems. An MG EMS is an advanced control system, consisting of multiple components and subsystems, capable of sensing grid conditions, monitoring and controlling the operation of an MG to maintain electricity delivery to critical loads during all MG operating modes. Before the operating day, the efficiency management function within EMS is implemented after the forecasting of loads and PV output profile along the operating day. The forecasting results are depicted as a scenario tree $\xi_s \in \Omega$ with a given probability density function $\pi_s, \forall s \in \Omega$. Using this scenario tree and the proposed multivariable nonlinear conversion loss models in Section III, a two-stage stochastic UC problem is formulated in Section IV and solved in Section V. The day-ahead UC solution is distributed among MGs, to schedule DGs along the operating day.

The physical meaning of two-stage stochastic UC is to schedule the diesel generators (DGs) within the MGs for the following operating day, as shown in Fig. 2, responding to the uncertainties from loads and renewable energy sources. With optimized unit commitment status of DGs, the power converted by the AC/DC and DC/DC converters, and power flow on DC networks can be adjusted by optimizing the voltage magnitudes, reducing power losses, and potentially reducing the fuel consumption and emissions. Moreover, when converter power loss was reduced through the proposed method, it also means less heat to be removed from the equipment, so it can relieve the burden of cooling system.

Remark 1: The energy management is to realize the optimal operation of MGs under various operating conditions, using monitoring, forecasting, and optimization functions. These functions always fall under the umbrella of decision-making problems. Within the optimization functions, there are day-ahead, intra-day, and real-time scheduling branches, where the unit commitment problems are widely formulated in the day-ahead and intra-day scheduling functions to schedule the resources with slow response characteristics, e.g., the start-up and shut-down of generators. In this work, the unit commitment problem is formulated to realize the day-ahead optimal operation of networked hybrid AC/DC microgrids (N-AC/DC-MGs), which is a function of energy management.

III. Multivariable Nonlinear Conversion Loss Models

Power loss models for bi-directional AC/DC and DC/DC converters are presented in this section. The models are formulated as multivariable nonlinear functions w.r.t power and voltage[1]. To reduce the computational cost, a linear multivariable surrogate model is adopted to approximate these nonlinear functions.

A. Power Loss Models of Bi-directional AC/DC Converters

The bi-directional AC/DC converters have two operating modes, i.e., rectification mode and inversion mode. Considering the conduction losses and switching losses under both modes, the conversion losses can be quantified by the following function [4]:

$$\begin{aligned} p_{\mathrm{L},c} = 6\{ & \frac{\sqrt{2}}{2} I_c V_{\mathrm{T},c} (\frac{1}{\pi} + \frac{m_c}{4}\cos(\theta_c)) \\ & + (\sqrt{2} I_c)^2 R_{\mathrm{T},c} (\frac{1}{8} + \frac{m_c}{3\pi}\cos(\theta_c)) \\ & + \frac{\sqrt{2}}{2} I_c V_{\mathrm{D},c} (\frac{1}{\pi} - \frac{m_c}{4}\cos(\theta_c)) \\ & + (\sqrt{2} I_c)^2 R_{\mathrm{D},c} (\frac{1}{8} - \frac{m_c}{3\pi}\cos(\theta_c)) \\ & + [\frac{1}{2\sqrt{\pi}} f_{\mathrm{S},c} h_{\mathrm{E,on},c} (\sqrt{2} I_c)^{k_{\mathrm{E,on},c}} \frac{\Gamma(\frac{k_{\mathrm{E,on},c}+1}{2})}{\Gamma(\frac{k_{\mathrm{E,on},c}}{2}+1)} \\ & + \frac{1}{2\sqrt{\pi}} f_{\mathrm{S},c} h_{\mathrm{E,off},c} (\sqrt{2} I_c)^{k_{\mathrm{E,off},c}} \frac{\Gamma(\frac{k_{\mathrm{E,off},c}+1}{2})}{\Gamma(\frac{k_{\mathrm{E,off},c}}{2}+1)} \\ & + \frac{1}{2\sqrt{\pi}} f_{\mathrm{S},c} h_{\mathrm{D},c} (\sqrt{2} I_c)^{k_{\mathrm{D},c}} \frac{\Gamma(\frac{k_{\mathrm{D},c}+1}{2})}{\Gamma(\frac{k_{\mathrm{D},c}}{2}+1)}] \frac{V_i^{\mathrm{DC}}}{\bar{V}_c} \} \\ & + (p_c^{\mathrm{rec}} + p_c^{\mathrm{inv}}) \eta_c \end{aligned} \tag{1}$$

where $I_c = \sqrt{2[(p_c^{\mathrm{rec}} - p_c^{\mathrm{inv}})^2 + q_c^2]/[3(V_i^{\mathrm{AC}})]^2}$, $m_c = 2\sqrt{V_{cd}^2 + V_{cq}^2}/V_i^{\mathrm{DC}}$, $\theta_c = \arctan(V_{cq}, V_{cd}) - \arctan(q_c, p_c^{\mathrm{inv}} - p_c^{\mathrm{rec}})$, $V_{cd} = \sqrt{2}V_{\mathrm{AC}} + r_{\mathrm{L},d} i_d - w L_c i_q$ and $V_{cq} = r_{\mathrm{L},d} i_q + w L_c i_d$. w is the angular frequency, i.e., 100π in this work. The first two lines are the conduction loss for IGBTs, the third and fourth lines are the conduction loss for anti-parallel diodes, the fifth line is IGBT switching on loss, the sixth line is IGBT switching off loss, the seventh line is the diode reverse recovery loss, and the last line is inductor losses. The detailed derivation can be found in [4].

In Eqn.(1), $p_c^{\mathrm{rec}} p_c^{\mathrm{inv}} = 0$, $p_c^{\mathrm{rec}} \geq 0$, and $p_c^{\mathrm{inv}} \geq 0$, indicate that the AC/DC can only operate in either rectification mode or inversion mode. $p_{\mathrm{L},c}$ is the function of $p_c^{\mathrm{inv}}, p_c^{\mathrm{rec}}, q_c, V_i^{\mathrm{DC}}$, under given parameters $V^{\mathrm{AC}}, f_{\mathrm{S},c}$, etc. The switching on, switching off and diode reverse recovery loss of AC/DC converter c depend linearly on the DC bus voltage V_i^{DC}, indicating the decrease of V_i^{DC} can reduce the power losses of AC/DC converters.

B. Power Loss Models of Bidirectional DC/DC Converters

For the low voltage applications in hybrid AC/DC MGs, the bi/directional DC-DC converter, using one half-bridge, is widely used for battery charging/discharging control. The high voltage side is connected to the DC bus and the low voltage side is connected to the battery, as shown in Fig. 2. For DC/DC converters, normally the inductor size is kept small to increase the converter power density, so the inductor current switching ripple can not be ignored. The gate PWM signals for the upper device T_1 and lower device T_2 are complementary to each other. It should be noted that when T_1 has a switch-on signal, the load current can flow through T_1 or D_1 which depends on the current direction. When the load current is positive (negative), it will flow through T_1 (D_1). The bi-directional DC/DC converter has three complete operation modes, i.e., buck, boost, and buck-boost. The power losses in different operation modes are given in this subsection.

[1]It should be noted that the power factor also plays an important role in conversion losses of AC/DC converters. In this work, the power factor of AC/DC converters is unity.

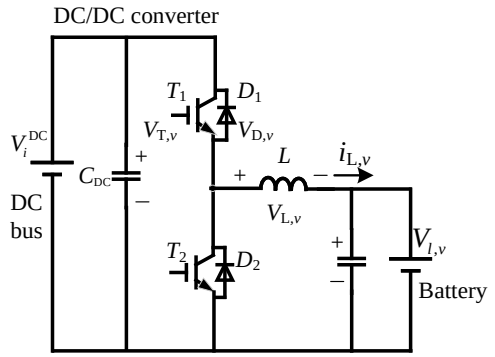

Fig. 2. Typical half-bridge DC/DC converters.V_i^{DC} refers to the DC bus voltage, where the DC/DC converter is integrated to. $V_{l,v}$ refers to the terminal voltage of ESS.

1) Power Losses in Buck Mode: The conversion losses of DC/DC converters in buck mode are given as follows:

$$\begin{aligned} p_{\text{L},v}^{\text{buck}} = & \underbrace{V_{\text{T},v} D_v i_{\text{L},v,\text{av}} + D_v (i_{\text{L},v,\text{av}}^2 + \frac{1}{12}\Delta i_{\text{L},v}^2) R_{\text{T},v}}_{\text{Conduction loss for device } T_1} \\ & + \underbrace{V_{\text{D},v}(1-D_v) i_{\text{L},v,\text{av}} + (1-D_v)(i_{\text{L},v,\text{av}}^2 + \frac{1}{12}\Delta i_{\text{L},v}^2) R_{\text{D},v}}_{\text{Conduction loss for device } D_2} \\ & + [\underbrace{f_{\text{S},v} h_{\text{E,on},v} i_{\text{L},v,\min}^{k_{\text{E,on},v}} + f_{\text{S},v} h_{\text{E,off},v} i_{\text{L},v,\max}^{k_{\text{E,off},v}}}_{\text{Switching loss for } T_1} \\ & + \underbrace{f_{\text{S},v} h_{\text{E,re},v} i_{\text{L},v,\min}^{k_{\text{E,re},v}}}_{\text{Reverse recovery loss for } D_2}] \frac{V_i^{\text{DC}}}{\bar{V}_v} \end{aligned} \tag{2}$$

where $i_{\text{L},v,\text{av}} = (p_v^{\text{ch}} - p_v^{\text{dc}})/V_{l,v}$, $D_v = V_{l,v}/V_i^{\text{DC}}$, $i_{\text{L},v,\max} = i_{\text{L},v,\text{av}} + \frac{\Delta i_{\text{L},v}}{2}$, and $i_{\text{L},v,\min} = i_{\text{L},v,\text{av}} - \frac{\Delta i_{\text{L},v}}{2}$.

2) Power Losses in Boost Mode: The conversion losses in boost mode can be derived using the same approach as in buck mode, as follows:

$$\begin{aligned} & p_{\text{L},v}^{\text{boost}} \\ & = \underbrace{V_{\text{T},v}(1-D_v)|i_{\text{L},v,\text{av}}| + (1-D_v)(i_{\text{L},v,\text{av}}^2 + \frac{1}{12}\Delta i_{\text{L},v}^2) R_{\text{T},v}}_{\text{Conduction loss for device } T_2} \\ & + \underbrace{V_{\text{D},v} D_v |i_{\text{L},v,\text{av}}| + D_v (i_{\text{L},v,\text{av}}^2 + \frac{1}{12}\Delta i_{\text{L},v}^2) R_{\text{D},v}}_{\text{Conduction loss for device } D_1} \\ & + [\underbrace{f_{\text{S},v} h_{\text{E,on},v} |i_{\text{L},v,\max}|^{k_{\text{E,on},v}} + f_{\text{S},v} h_{\text{E,off},v} |i_{\text{L},v,\min}|^{k_{\text{E,off},v}}}_{\text{Switching loss for } T_2} \\ & + \underbrace{f_{\text{S},v} h_{\text{E,re},v} |i_{\text{L},v,\max}|^{k_{\text{E,re},v}}}_{\text{Reverse recovery loss for } D_1}] \frac{V_i^{\text{DC}}}{\bar{V}_v} \end{aligned} \tag{3}$$

3) Power Losses in Buck-boost Mode: The conversion losses in buck-boost mode are shown as follows:

$$\begin{aligned} & p_{\text{L},v}^{\text{buck-boost}} \\ & = \underbrace{V_{\text{D},v} D_v \frac{|i_{\text{L},v,\min}|}{\Delta i_L} \frac{|i_{\text{L},v\,\min}|}{2} + \frac{D}{3}\frac{|i_{\text{L},v,\min}|^3}{\Delta i_L} R_{\text{D},v}}_{\text{Conduction loss for diode } D_1} \\ & + \underbrace{V_{\text{T},v} D_v \frac{|i_{\text{L},v,\max}|}{\Delta i_{\text{L,v}}} \frac{|i_{\text{L},v,\max}|}{2} + \frac{D}{3}\frac{|i_{\text{L},v,\max}|^3}{\Delta i_{\text{L},v}} R_{\text{T},v}}_{\text{Conduction loss for device } T_1} \\ & + \underbrace{V_{\text{D},v}(1-D_v) \frac{|i_{\text{L},v,\max}|}{\Delta i_{\text{L},v}} \frac{|i_{\text{L},v,\max}|}{2} + \frac{1-D}{3}\frac{|i_{\text{L},v,\max}|^3}{\Delta i_{\text{L},v}} R_{\text{D},v}}_{\text{Conduction loss for diode } D_2} \\ & + \underbrace{V_{\text{T},v}(1-D_v) \frac{|i_{\text{L},v,\min}|}{\Delta i_{\text{L},v}} \frac{|i_{\text{L},v,\min}|}{2} + \frac{1-D_v}{3}\frac{|i_{\text{L},v,\min}|^3}{\Delta i_{\text{L},v}} R_{\text{T},v}}_{\text{Conduction loss for device } T_2} \\ & + [\underbrace{f_{\text{S},v} h_{\text{E,off},v} |i_{\text{L},v,\max}|^{k_{\text{E,off},v}}}_{\text{Switch off power of } T_1} + \underbrace{f_s h_{\text{E,off},v} |i_{L\,\min}|^{k_{\text{E,off},v}}}_{\text{Switching off losses of } T_2}] \frac{V_i^{\text{DC}}}{\bar{V}_v} \end{aligned} \tag{4}$$

The power losses of DC/DC converter v are $p_{\text{L},v} := p_{\text{L},v}^{\text{buck}} + p_{\text{L},v}^{\text{boost}} + p_{\text{L},v}^{\text{buck-boost}} + \eta_v |p_v^{\text{ch}} - p_v^{\text{dc}}|$. The DC/DC converter can only operate at one of three modes. $p_{\text{L},v}$ depends on the $p_v^{\text{ch}}, p_v^{\text{dc}}, V_i^{\text{DC}}$ under given parameters $D_v, R_{\text{D},v}, R_{\text{T},v}, f_{\text{S},v}, h_{\text{E,off},v}, k_{\text{E,off},v}$, etc. Detailed derivations on Eqns.(2)-(4) are shown in Appendix A.

Remark 2: When V^{AC}, V_i^{DC} and V_v are fixed, the conversion losses of AC/DC and DC/DC converters mainly depend on current, as $I_c = \sqrt{2[(p_c^{\text{rec}} - p_c^{\text{inv}})^2 + q_c^2]/[3(V_i^{\text{AC}})]^2}$ and $i_{\text{L},v,\text{av}} = (p_v^{\text{ch}} - p_v^{\text{dc}})/V_i^{\text{DC}}$. The multivariable nonlinear conversion losses can be reduced to classical univariate nonlinear conversion loss models [5], [13].

C. Linear Surrogate Models of Conversion Losses

As shown in Eqns. (2)-(4), the conversion losses are multivariable non-convex nonlinear functions w.r.t. the power and voltage V_i^{DC}. To reduce the computational cost, the triangle approximation based piece-wise linear function [35] is adopted to reformulate these loss functions into the following linear

surrogate models:

$$\begin{aligned}
&\sum_{i=1}^{n_x}\sum_{j=1}^{m_y}\alpha_{ij}=1\\
&x=\sum_{i=1}^{n_x}\sum_{j=1}^{m_y}\alpha_{ij}x_i\\
&y=\sum_{i=1}^{n_x}\sum_{j=1}^{m_y}\alpha_{ij}y_j\\
&f=\sum_{i=1}^{n_x}\sum_{j=1}^{m_y}\alpha_{ij}f(x_i,y_j)\\
&\sum_{i=1}^{n_x-1}\sum_{j=1}^{m_y-1}(h_{ij}^u+h_{ij}^l)=1\\
&\alpha_{ij}\le h_{ij}^u+h_{ij}^l+h_{i,j-1}^u+h_{i-1,j-1}^l+h_{i-1,j-1}^u+h_{i-1,j}^l,\\
&\forall i=1,...,n_x,j=1,...,m_y
\end{aligned}\tag{5}$$

where α_{ij} is a special order set 3. $x:=\{p_c^{\text{rec}}-p_c^{\text{inv}},p_v^{\text{ch}}-p_v^{\text{dc}}\}$, $y:=\{V_i^{\text{DC}}\}$, and $f:=\{p_{\text{L},c},p_{\text{L},v}\}$.

IV. Two-stage Stochastic Unit Commitment under Linear Surrogate Losses

With the linear surrogate conversion loss model (5), a dynamic OPF problem is formulated as a mixed-integer second-order conic programming (MI-SOCP) problem. This problem is further treated as the recourse for the two-stage stochastic UC problem under stochastic uncertainties.

A. Two-stage Stochastic Unit Commitment Problem

The UC problem for N-AC/DC-MGs has been formulated as the following two-stage stochastic programming problem:

$$\min_{\mathbf{x}\in\mathcal{X}} f(\mathbf{x})+\sum_{\xi_s\in\Omega}\pi_s[\mathcal{Q}(\mathbf{x},\xi_s)] \tag{6}$$

$$\mathcal{Q}(\mathbf{x},\xi_s)=\min_{\mathbf{y}_s\in\mathcal{Y}(\mathbf{x},\xi_s)} g(\mathbf{y}_s) \tag{7}$$

where $\mathbf{x}:=\{\alpha_g^t,\beta_g^t,I_g^t,\forall g,t\}$ is a binary vector, $\mathcal{X}$ is the first-stage constraint set. Ω is the uncertainty set of rand vector $\xi_s:=\{p_{\text{D},i}^{\text{AC},t},p_{\text{D},i}^{\text{DC},t},p_{\text{PV},i}^t,\forall i,t\}$, including the loads and PV output[2]. $\mathcal{Q}(\mathbf{x},\xi_s)$ is the dynamic OPF with given $\mathbf{x}$ and ξ_s, as an MI-SOCP problem, where $\mathbf{y}_s:=\{p_{\text{UG},i}^t,p_g^t,p_{\text{L},i}^{\text{rec},t},p_{\text{C},i}^{\text{inv},t},p_{\text{ESS},i}^{\text{dc},t},p_{\text{ESS},i}^{\text{c},t},p_{\text{L},i}^{\text{inv},t},p_{\text{C},i}^{\text{inv},t},p_{\text{MG},i}^t,e_{\text{ESS},i}^t,p_{\text{L},i}^{\text{ch},t},p_{\text{L},i}^{\text{dc},t},I_{\text{ESS},i}^{\text{dc},t},I_{\text{ESS},i}^{\text{c},t},I_{\text{C},i}^{\text{rec},t},I_{\text{C},i}^{\text{inv},t},l_{ij}^t,p_{ij}^t,v_i^t,\forall i,ij,g,t\}$ is a mixed-integer vector, due to existence of the binary variables $I_{\text{ESS},i}^{\text{dc},t},I_{\text{ESS},i}^{\text{ch},t},I_{\text{C},i}^{\text{rec},t}$ and $I_{\text{C},i}^{\text{inv},t}$. $\mathcal{Y}(\mathbf{x},\xi_s)$ is a convex set, where the power losses $p_{\text{L},i}^{\text{rec},t}$, $p_{\text{L},i}^{\text{inv},t}$, $p_{\text{L},i}^{\text{ch},t}$ and $p_{\text{L},i}^{\text{dc},t}$ are depicted by their corresponding linear surrogate models.

[2]Numerous methods can be used to generate the scenario set and assign their corresponding probability density functions, e.g., scenario generation and reduction [36].

B. First-stage Optimization

The first-stage is to minimize the start-up and shut-down cost of DGs, by optimizing their start-up, shut-down and operating status, as follows:

$$f(\mathbf{x})=\sum_{t\in\mathcal{T}}\sum_{g\in\mathcal{G}}(c_{\text{U},g}\alpha_g^t+c_{\text{D},g}\beta_g^t) \tag{8}$$

The first-stage constraint set $\mathcal{X}$ includes the operating status transition, minimum start-up duration,maximum start-up duration, minimum shut-down duration and initial condition constraints, which are referred to [9] for details.

C. Second-stage Optimization

The second-stage optimization is to minimize the total power losses, via optimizing the power output of DGs and ESSs, the voltage of AC/DC converters and DC/DC converters, etc., as the following dynamic OPF problem:

$$\begin{aligned}
g(\mathbf{y})=\sum_{t\in\mathcal{T}}\{\sum_{i\in\mathcal{M}}[\sum_{c\in\mathcal{C}_i}(p_{\text{L},c}^{\text{rec},t}+p_{\text{L},c}^{\text{inv},t})\\
+\sum_{v\in\mathcal{V}_i}(p_{\text{L},v}^{\text{dc},t}+p_{\text{L},v}^{\text{ch},t})]+\sum_{ij\in\mathcal{E}}R_{ij}l_{ij}^t\}
\end{aligned}\tag{9}$$

The second-stage constraint set $\mathcal{Y}(\mathbf{x},\xi)$ includes both MGs and distribution systems constraints. For each MG i, the constraints, including the AC and DC bus power balance constraints, are listed as follows:

$$\underline{P}_g I_g\le p_g^t\le\bar{P}_g I_g,\forall g,t \tag{10}$$

$$-R_g\Delta t\le p_g^t-p_g^{t-\Delta t}\le R_g\Delta t,\forall g,t \tag{11}$$

$$e_{\text{ESS},i}^t=e_{\text{ESS},i}^{t-\Delta t}+(p_{\text{ESS},i}^{\text{ch},t}-p_{\text{L},i}^{\text{ch},t}-p_{\text{ESS},i}^{\text{dc},t}+p_{\text{L},i}^{\text{dc},t})\Delta t,\forall i,t \tag{12}$$

$$0\le p_{\text{ESS},i}^{\text{dc},t}\le S_{\text{ESS},i}I_{\text{ESS},i}^{\text{dc},t},\forall i,t \tag{13}$$

$$0\le p_{\text{ESS},i}^{\text{ch},t}\le S_{\text{ESS},i}I_{\text{ESS},i}^{\text{ch},t},\forall i,t \tag{14}$$

$$I_{\text{ESS},i}^{\text{ch},t}+I_{\text{ESS},i}^{\text{dc},t}\le 1,\forall i,t \tag{15}$$

$$\underline{E}_{\text{ESS},i}\le e_{\text{ESS},i}^t\le\bar{E}_{\text{ESS},i},\forall i,t \tag{16}$$

$$0\le p_{\text{C},i}^{\text{rec},t}\le S_{\text{C},i}I_{\text{C},i}^{\text{rec},t},\forall i,t \tag{17}$$

$$0\le p_{\text{C},i}^{\text{inv},t}\le S_{\text{C},i}I_{\text{C},i}^{\text{inv},t},\forall i,t \tag{18}$$

$$I_{\text{C},i}^{\text{rec},t}+I_{\text{C},i}^{\text{inv},t}\le 1,\forall i,t \tag{19}$$

$$0\le p_{\text{UG},i}^t\le\bar{P}_{\text{UG},i},\forall i,t \tag{20}$$

The AC and DC bus power balance constraints are referred to [2]. The generator output and ramp constraints are given in Eqn.(10) and (11), respectively. The energy and power related constraints of battery ESSs are depicted by Eqns.(12)-(16). The power conversion constraints on the interlinking converters, i.e., a type of AC/DC converter, are illustrated in Eqns.(17)-(19). The power exchange between the MG and utility grid is limited by Eqn.(20). In Eqns.(**??**),(**??**), and (12), the power losses, i.e., $p_{\text{L},i}^{\text{rec},t}$, $p_{\text{L},i}^{\text{inv},t}$, $p_{\text{L},i}^{\text{ch},t}$ and $p_{\text{L},i}^{\text{dc},t}$ are non-convex w.r.t voltage and converter power, as shown in Eqns.(1), (2), (3) and (4). Using the linear surrogate models

(5), these loss functions are depicted by a set of linear constraints with mix-integer variables.

Following the branch power flow [37], the constraints for DC distribution systems within the N-AC/DC-MGs are given as follows:

$$\sum_{k:k\to j} p_{jk}^t = \sum_{i:i\to j} (p_{ij}^t - R_{ij} l_{ij}^t) + p_{\text{MG},j}^t, \forall j, t \tag{21}$$

$$v_j^t - v_k^t = 2R_{jk}p_{jk}^t - R_{jk}^2 l_{jk}^t, \forall jk, t \tag{22}$$

$$v_j^t l_{jk}^t \geq p_{jk}^{t,2}, \forall jk, t \tag{23}$$

$$0 \leq l_{jk}^t \leq \bar{l}_{jk}, \forall jk, t \tag{24}$$

$$\underline{v}_i \leq v_i^t \leq \bar{v}_i, \forall i, t \tag{25}$$

where $l_{jk}(t) := I_{jk}^2(t)$, $I_{jk}(t)$ is the current in line $j \to k$, $v_j(t) := (V_j^{\text{DC}}(t))^2$.

The power balance constraint at each DC bus is shown in Eqn.(21), the Ohm's law is shown in Eqn.(23), and power definition, i.e., $v_j^t l_{jk}^t = p_{jk}^{t,2}$, is relaxed in Eqn.(23). The exactness of the relaxation has been discussed in [2], [37] for DC distribution networks under given conditions. e.g., with the uniform upper boundary of voltage magnitudes.

Remark 3: In Eqn.(25), $\underline{v}_i$ is limited by the $m_c < 1$, indicating $2\sqrt{V_{cd}^2 + V_{cq}^2}/V_i^{\text{DC}} \leq 1$ and $\underline{v}_i \geq 2\sqrt{V_{cd}^2 + V_{cq}^2}$.

As shown in Eqns.(**??**)-(23), the $\mathcal{Q}(\mathbf{x}, \xi_s)$ is an MI-SOCP problem with linear surrogate models (5). For further analysis, the UC problem can be represented as the following compact model:

$$\begin{aligned} \min_{\mathbf{x}} \ & f(\mathbf{x}) + \sum_{s=1}^{|\Omega|} \pi_s g(\mathbf{y}_s) \\ \text{s.t.} \ & \mathbf{A}\mathbf{x} \leq \mathbf{b}, \mathbf{x} \in \mathbb{B}^{n_1} \end{aligned} \tag{26}$$

$$\begin{aligned} \mathcal{Q}(\mathbf{x}, \xi_s) = \min_{\mathbf{y}_s} \ & g(\mathbf{y}_s) \\ \text{s.t.} \ & \mathbf{T}\mathbf{x} + \mathbf{W}\mathbf{y}_s \leq \mathbf{b}_s(\xi_s), \\ & \mathbf{y}_s \in \mathcal{C}, \mathbf{y}_s \in \mathbb{B}^{n_2} \times \mathbb{R}^m \end{aligned} \tag{27}$$

where $\mathcal{C}$ is the conic constraint set of power definition (23).

V. Solution Methods

In this section, an improved Benders decomposition algorithm is adopted to solve problem (26). The improved linear cuts are integrated into the multicuts Benders decomposition algorithm with finite iteration convergence guarantee.

Problem (26) is a large scale MI-SOCP problem, with the increasing number of scenarios in Ω. For fixed $\mathbf{x}$, the subproblems $\mathcal{Q}(\mathbf{x}, \xi_s)$ can be solved in parallel, reducing the computational cost significantly. Due the existence of binary variables in $\mathbf{y}_s$, the classical duality based Benders decomposition should be improved, where the improved linear cuts can be adopted to approximate the mixed recourse [34].

For the given first-stage solution $\mathbf{x}^*$, the following convex optimization problem is solved to derive the Lagrange multiplier of the equal constraint $\hat{\mathbf{x}} = \mathbf{x}^*$.

$$\begin{aligned} \hat{\mathcal{Q}}(\hat{\mathbf{x}}, \xi_s) = \min_{\hat{\mathbf{x}}, \mathbf{y}_s} \ & g(\mathbf{y}_s) \\ \text{s.t.} \ & \mathbf{T}\hat{\mathbf{x}} + \mathbf{W}\mathbf{y}_s \leq \mathbf{b}_s(\xi_s), \\ & \mathbf{y}_s \in \mathcal{C}, \\ & \hat{\mathbf{x}} = \mathbf{x}^* : (\lambda_s) \end{aligned} \tag{28}$$

Problem (28) might be infeasible for given $\mathbf{x}^*$, indicating the formulated recourse is not complete. The following problem is introduced to relax the original second-stage problem via introducing load shedding on both AC bus and DC bus, formulating a complete recourse problem:

$$\begin{aligned} \check{\mathcal{Q}}(\hat{\mathbf{x}}, \xi_s) = \min_{\hat{\mathbf{x}}, \mathbf{y}_s, p_{\text{S},i}^{\text{AC},t}, p_{\text{S},i}^{\text{DC},t}} \ & g(\mathbf{y}_s) + \sum_{t\in\mathcal{T}} \sum_{i\in\mathcal{M}} c_{\text{VOLL}} (p_{\text{S},i}^{\text{AC},t} + p_{\text{S},i}^{\text{DC},t}) \\ \text{s.t.} \ & \text{Eqns.}(\textbf{??}), (10) - (23) \\ & p_{\text{UG},i}^t + \sum_{g\in\mathcal{G}_i} p_g^t + p_{\text{L},i}^{\text{rec},t} = p_{\text{D},i}^{\text{AC},t} + p_{\text{C},i}^{\text{rec},t} - p_{\text{S},i}^{\text{AC},t}, \forall i, t \\ & p_{\text{ESS},i}^{\text{dc},t} - p_{\text{ESS},i}^{\text{ch},t} + p_{\text{L},i}^{\text{inv},t} + p_{\text{PV},i}^t = \\ & \qquad p_{\text{D},i}^{\text{DC},t} + p_{\text{C},i}^{\text{inv},t} + p_{\text{MG},i}^t - p_{\text{S},i}^{\text{DC},t}, \forall i, t \\ & 0 \leq p_{\text{S},i}^{\text{DC},t} \leq p_{\text{D},i}^{\text{AC},t} \\ & 0 \leq p_{\text{S},i}^{\text{DC},t} \leq p_{\text{D},i}^{\text{DC},t} \\ & \mathbf{y}_s \in \mathcal{C}, \\ & \hat{\mathbf{x}} = \mathbf{x}^* : (\lambda_s) \end{aligned} \tag{29}$$

With the obtained λ_s, the following problem is proposed to estimate the lower boundary of $\hat{\mathcal{Q}}(\mathbf{x}^*, \xi_s)$ under ξ_s:

$$\begin{aligned} \mathcal{Q}'(\tilde{\mathbf{x}}, \xi_s) = \min_{\tilde{\mathbf{x}}, \mathbf{y}_s} \ & [g(\mathbf{y}_s) - \lambda_s^{\text{T}} \tilde{\mathbf{x}}] \\ \text{s.t.} \ & \mathbf{T}\tilde{\mathbf{x}} + \mathbf{W}\mathbf{y}_s \leq \mathbf{b}_s(\xi_s), \\ & \mathbf{y}_s \in \mathcal{C}, \\ & \tilde{\mathbf{x}} \in \mathbb{R}^{n1}, \mathbf{y}_s \in \mathbb{B}^{n_2} \times \mathbb{R}^m \end{aligned} \tag{30}$$

The obtained λ_s and $\hat{\mathcal{Q}}(\mathbf{x}^*, \xi_s)$ can be used to formulate the dual cut under ξ_s:

$$\theta_s \geq \lambda_s^{\text{T}} \mathbf{x} + \mathcal{Q}'(\tilde{\mathbf{x}}, \xi_s) \tag{31}$$

The linear cut (31) is further integrated into the following master problem as a constraint:

$$\begin{aligned} \min_{\mathbf{x}, \theta_s} \ & f(\mathbf{x}) + \sum_{s=1}^{N} \pi_s \theta_s \\ \text{s.t.} \ & \mathbf{A}\mathbf{x} \leq \mathbf{b}, \\ & \theta_s \geq \lambda_s^{l,\text{T}} \mathbf{x} + \mathcal{Q}'^l(\tilde{\mathbf{x}}, \xi_s), l = 1, ...k \\ & \mathbf{x} \in \mathbb{B}^{n_1}, \theta_s \in \mathbb{R}, \forall s \end{aligned} \tag{32}$$

The detailed solution procedure is given in Algorithm 1.

Theorem 1: Algorithm 1 converges in finite iterations.

Proof: Using problem (29), there always exits an equivalent complete recourse counterpart for problem (26). Given that the first stage decision variables are binary, Algorithm 1 converges in finite iterations, based on Theorem 4 in [34].

Algorithm 1: Improved Benders decomposition algorithm

Data: $\mathcal{X}$,$\mathcal{Y}(\mathbf{x},\xi_s)$, $\xi_s,\forall s$, and $n_{\max}$
Result: $\mathbf{x}$, $\mathbf{y}_s,\forall s$

Set $LB^0 = -\inf$, $UB^0 = \inf$ and $n = 1$
while $n \leq n_{max}$ **do**
  Derive an optimal solution $\mathbf{x}^n$ by solving (32)
  if *problem (32) is infeasible* **then**
    Terminate
  else
    Update $LB^n = \max\{LB^{n-1}, \text{objective value of MP}\}$
    for $s \in \Omega$
    if *if (28) is feasible* **then**
      Derive λ_s by solving (28)
    else
      Derive λ_s by solving (29)
    end
      Derive $\mathcal{Q}'(\tilde{\mathbf{x}},\xi_s)$ by solving (30)
      Derive cuts by solving (31)
    end
    Update $UB^n = \min\{f(\mathbf{x}^m) + \sum_{s\in\Omega}\mathcal{Q}'(\tilde{\mathbf{x}},\xi_s), UB^{n-1}\}$
    if $(UB^m - LB^m)/\max(UB^m, LB^m) \leq \epsilon$ **then**
      Return $\mathbf{x}^*, \mathbf{y}_s^*$ and terminate
    else
      Add cuts (31) to the master problem (32)
      Update $m = m + 1$
    end
  end
end

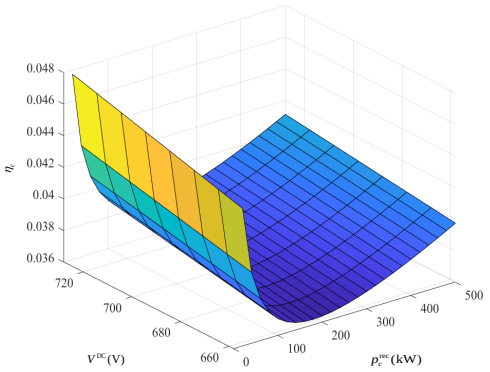

Fig. 3. Conversion losses of AC/DC converters under different voltage magnitude and power levels. The power factor is set to unity. $\eta_c = P_{\text{L},c}/(|p_c^{\text{inv}} - p_c^{\text{rec}}|)$.

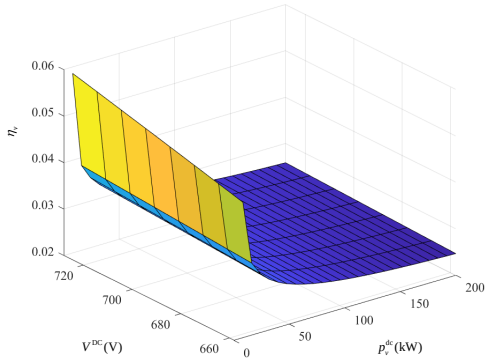

Fig. 4. Conversion losses of DC/DC converters under different voltage magnitude and power levels. $\eta_v = P_{\text{L},v}/(|p_v^{\text{dc}} - p_v^{\text{ch}}|)$.

VI. Case Study

To verify the effectiveness of the proposed stochastic management scheme under multivariable nonlinear power loss models, the case studies are conducted on a single hybrid AC/DC MGs and networked hybrid AC/DC MGs in this section.

A. Case Description

The case study is tested on a three-bus mesh DC network with three hybrid AC/DC MGs. The output of PV and loads are assumed to follow normal distributions, which can be obtained by the stochastic forecasting techniques [38]. The detailed scenario tree Ω and configuration of each MG are referred to [2]. The parameters of the DGs are obtained from [21]. The parameters of bi-directional AC/DC and DC/DC converters are obtained from the datasheet of SKM1400GB12P4. The power losses of bi-directional AC/DC and DC converters under different voltage and power are shown in Figs.3 and 4. There are 100 scenarios in Ω. The stopping criteria are set to 1e-2 within Algorithm 1. m_x and n_y are set to 26 and 8, respectively. CPLEX is adopted in Algorithm 1. The detailed parameters can be accessed via [39].

The following cases are conducted on the hybrid AC/DC MGs and N-AC/DC-MGs. The comparison among Cases I-III is to verify the effectiveness of the proposed energy management with optimized voltage magnitudes for hybrid AC/DC MGs. The results of Cases IV-VI are to verify the performance of the proposed energy management for N-AC/DC-MGs, where the voltages of converters are correlated by the power flow on DC networks. Cases VII-IX are conducted to show the scalability of the proposed scheme.

1) Case I, Isolated MGs with fixed conversion efficiency[3].
2) Case II, Isolated MGs with fixed voltage magnitudes[4].
3) Case III, Isolated MGs with proposed conversion loss models.
4) Case IV, Networked MGs with fixed conversion losses.
5) Case V, Networked MGs with fixed voltage magnitudes.
6) Case VI, Networked MGs with proposed conversion loss models.
7) Case VII, Larger networked MGs with fixed conversion losses.
8) Case VIII, Larger networked MGs with fixed voltage magnitudes.

[3] $\eta_c = 0.04$ and $\eta_v = 0.025$.
[4] $\overline{V}_i^{\text{DC}}$ is fixed, and the conversion losses are approximated by a univariate quadratic function w.r.t current.

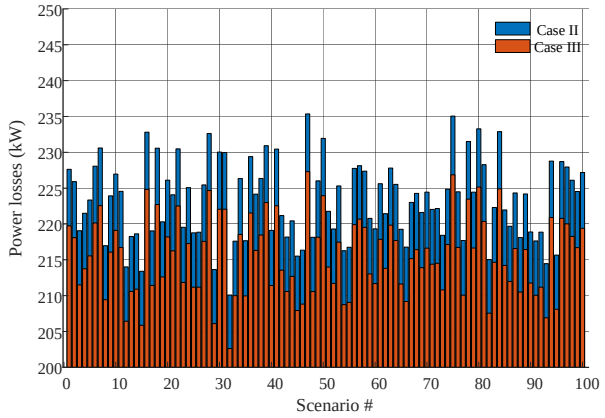

Fig. 5. Expected power losses under different scenarios in Cases II and III.

9) Case IX, Larger networked MGs with proposed conversion loss models.

B. Simulation Result of Hybrid AC/DC MGs

TABLE I
POWER LOSSES UNDER DIFFERENT CASES FOR ISOLATED HYBRID AC/DC MGS

	Case I	Case II	Case III
Expected power losses(kW)	234.45	223.28	215.52
Actual power losses(kW)	213.55	215.91	215.20

The expected and actual[5] power losses under Case I, II, and III are shown in Tab.I, and the total power losses under different scenarios in Case II and Case III are shown in Fig. 5. As shown in Tab.I, the total power losses are reduced by 4.76%, in comparison with the fixed conversion efficiency. The total power losses have been further reduced by 3.48% when the DC bus voltage can be adjusted in Case III. What is more, the total power losses can always be decreased within the same scenario, as illustrated by Fig. 5. It indicates the loss minimization problem is robust under the disturbance from renewable energy sources and loads.

The DC bus voltage magnitude, $V^{\mathrm{DC},t,s}$, within different scenarios in Case III is shown in Fig. 6. As it can be observed from Fig. 6, the DC bus voltage magnitude can optimized, i.e., decreasing from 700V to [660.83V, 679.78V] in Fig. 6. Considering the conversion efficiency in Fig. 3, the reduction of DC bus voltage can decrease the conversion losses, as a direct result of the conversion losses model 5 w.r.t. voltage.

The power flow on the bi-directional AC/DC converter under Case III is shown in Fig. 7. As shown in Fig. 7, the bi-directional converters are always working on the rectifying mode, i.e., converting power from AC side to DC side. During 10:00-18:00, the expected DC bus voltage is slightly increased to 679.78 V. There is no power converted from AC side to DC side, avoiding increasing the conversion losses.

[5]The actual power losses are calculated without any linearized model.

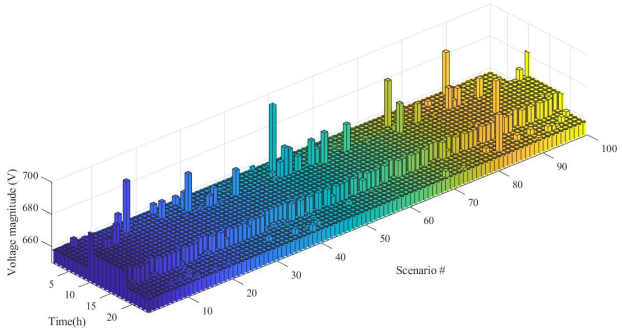

Fig. 6. Voltage magnitude of DC bus under Case III.

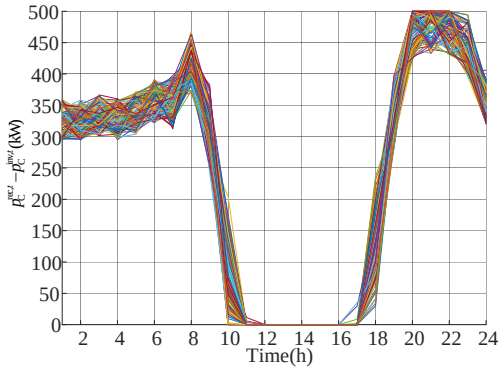

Fig. 7. Power flow on bi-directional AC/DC converter under Case III.

The box plot of the relative error of power losses of AC/DC converters, i.e., $P_{\mathrm{L},c} - \bar{P}_{\mathrm{L},c}$, where $\bar{P}_{\mathrm{L},c}$ is the actual power losses, is given in Fig. 8. The relative error is within the interval [-0.05 kW, 0.15 kW], and the total expected relative error is 0.32 kW, as shown in Tab. I. The largest errors appear during 10:00-10:59 and 18:00-18:59, where the power flow on the bi-directional AC/DC converter is less than 20 kW, as shown in Fig.7. Together with the conversion losses in Fig. 3, its nonlinearity can be approximated by the surrogate model (5).

C. Simulation Result of Networked Hybrid AC/DC MGs

The expected power losses for networked hybrid AC/DC MGs under Cases IV, V, and VI are given in Tab. II. The total power losses are reduced by 7.88% when the univariate nonlinear cost is adopted in Case V. Event the relative error of Cases V and VI are almost the same, the total power losses are further reduced to 318.80 kW, as the DC bus voltage can be adjusted in Case VI. The proposed stochastic UC problem can manage prevalent conversion loss models, and the proposed multivariable nonlinear conversion loss models might lead to more accurate results. It should be noted that, when the DC networks constraints (21)-(25) are omitted, the power losses can be further reduced to 310.86 kW, indicating the necessity to consider the physical law among voltages within N-AC/DC MGs.

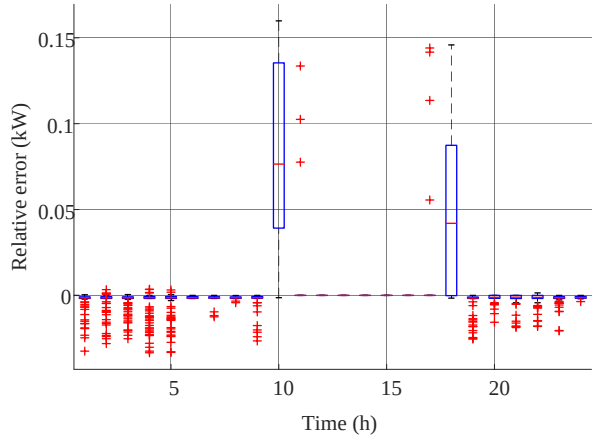

Fig. 8. Box plot of relative error of AC/DC conversion losses under Case III.

TABLE II
POWER LOSSES UNDER DIFFERENT CASES FOR NETWORKED HYBRID AC/DC MGS

	Case IV	Case V	Case VI
Expected power losses(kW)	364.37	335.64	318.80
Actual power losses(kW)	358.03	358.09	335.51

The unit commitment status of DGs within MGs is given in Fig. 9. All DGs within MG 2 and MG 3 are online, to reduce the energy imported to MGs 1, reducing the transmission losses. With the accurate conversion losses estimated in Tab. II, the unit in MG 1 is shut down during 23:00-23:59 in Case VI. These results reveal that the conversion losses can affect the commitment status using the proposed UC strategy.

The expected voltage magnitudes of DC buses within networked hybrid AC/DC MGs are given in Figs.10, respectively. As illustrated by Fig. 10, the expected voltage magnitudes vary along the operating day, and there exist voltage magnitude differences between MGs. According to (21)-(22), these voltage differences can result in power injection to the DC networks, enabling energy sharing among MGs.

The relation between the power losses and the number of piece-wise blocks under case VI is given in Fig. 11. As it can be observed within this figure, the increase in the scale of blocks results in a decrease in expected power losses, as the larger blocks within the operating regions can always be approximated by the smaller blocks. The fallen of the block scale leads to the decrease in the number of decision variables in the recourse problem (7), from 181440 to 17280. However, the actual power losses might be allocated even with a few blocks. It indicates the computational cost and piece-wise construction methods should be carefully designed [14].

D. Simulation Result of Larger Test Cases

To further evaluate the scalability of the proposed energy management, further case studies are conducted using different types of power losses models. In these cases, three hybrid

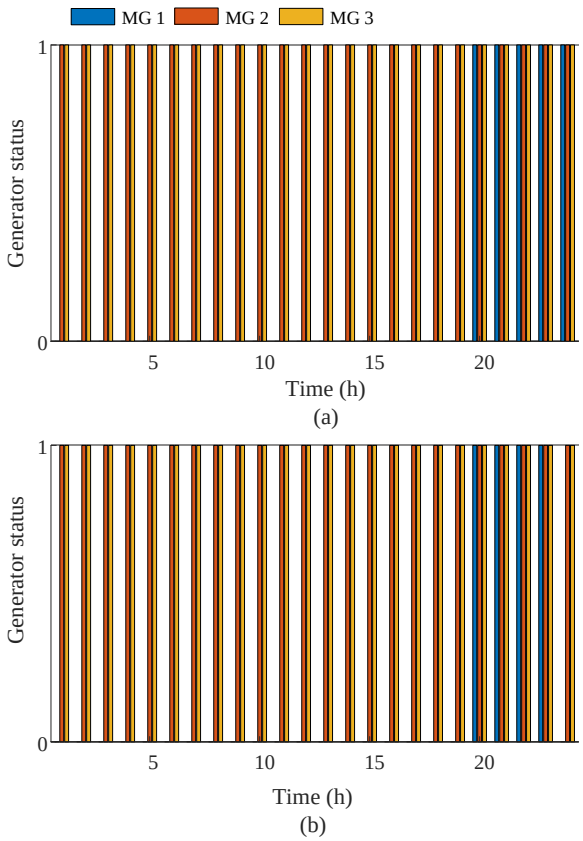

Fig. 9. Unit commits of DGs.(a) Commitment status of DGs in Cases IV and V. (b) Commitment status of DGs in Case VI.

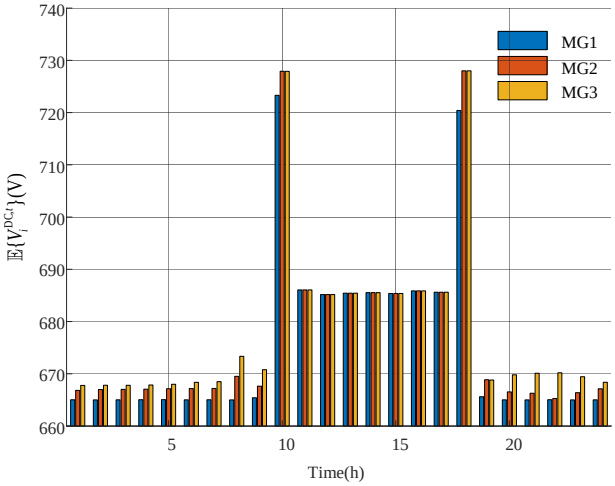

Fig. 10. DC bus voltage under Case VI.

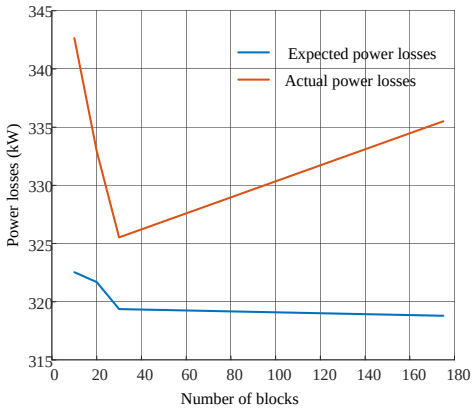

Fig. 11. Relation between the power losses and number of piece-wise blocks of model (5) under Case VI. The number of blocks is $(n_x - 1)(m_y - 1)$.

TABLE III
POWER LOSSES UNDER DIFFERENT CASES FOR NETWORKED HYBRID AC/DC MGS WITH 33 DC BUSES

	Case VII	Case VIII	Case IX
Expected power losses (kW)	899.01	879.68	852.23
Actual power losses (kW)	869.28	864.58	858.37

AC/DC MGs are interconnected by a 33-bus distribution system, similar to the topology within Ref. [40], using the same parameters as the IEEE-33 bus test system. Within the DC networks, the loads are interconnected to different buses. The power balance equation (21) should be extended, i.e., $\sum_{k:k\to j} p^t_{jk} = \sum_{i:i\to j}(p^t_{ij} - R_{ij} l^t_{ij}) + p^t_{\text{MG},j} - p^t_{\text{D},j}, \forall j, t$. The expected power losses using different conversion losses models are given in Tab. III. It can be found that the power losses are minimal using the proposed surrogate model (5), where the voltage can be optimized. The relative errors of power lossses under case IX are within [0, 0.15 kW], which is much smaller than the relative errors under case VIII. Due to page limitations, the rest of the results can be accessed by the IEEE dataport [39].

VII. CONCLUSION

Novel multivariable nonlinear models have been proposed for the bi-directional AC/DC and DC/DC conversion losses, where voltage can be optimized within the N-AC/DC MGs. The models are approximated by linear surrogate models and incorporated into the two-stage stochastic UC problem, as a mixed-integer recourse. It has been further solved by an Benders decomposition algorithm with finite iteration convergence property. The same multivariable conversion loss model for bidirectional AC/DC and DC/DC converters is used for the three different energy management strategies to guarantee fair comparison.

The results indicate that the power losses are reduced by introducing univariate nonlinear conversion loss models and can be further decreased by proposed multivariable nonlinear conversion loss models when the DC bus voltage can be optimized. The stochastic management scheme can improve operational efficiency under uncertainties. It has been proved that with more accurate conversion loss models embedded within the EMS, the output commands from the EMS will lead to more efficient system operation and thus save more energy in the networked system.

APPENDIX A
POWER LOSS MODELS FOR BI-DIRECTIONAL DC/DC CONVERTERS

For the bi-directional DC/DC converter using one half-bridge topology shown in Fig. 2, the power loss models under buck, boost, and buck-boost modes are derived.

The duty cycle for the upper device T_1 is D_v, whereas the duty cycle for T_2 is (1-D_v). The inductor current ripple $\Delta i_{\text{L},v}$[6] can be calculated as follows:

$$\Delta i_{\text{L},v} = \frac{(1-D_v)T_S}{L_v} V_{l,v} = \frac{(1-D_v)V_{l,v}}{L f_{\text{S},v}} \tag{33}$$

The average inductor current $i_{\text{L},v,\text{av}}$ can be calculated based on the charging power at the battery side as follows:

$$i_{\text{L},v,\text{av}} = \frac{p^{\text{ch}}_v - p^{\text{dc}}_v}{V_{l,v}} \tag{34}$$

The maximum and minimum inductor currents can be calculated as follows:

$$\begin{aligned} i_{\text{L},v,\max} &= i_{\text{L},v,\text{av}} + \frac{\Delta i_{\text{L},v}}{2} \\ i_{\text{L},v,\min} &= i_{\text{L},v,\text{av}} - \frac{\Delta i_{\text{L},v}}{2} \end{aligned} \tag{35}$$

During the buck operation mode, as shown in Fig. 12, the inductor current is always positive which means $i_{\text{L},v,\max} \geq i_{\text{L},v,\min} \geq 0$. The device T_1 and D_2 are conducting during inductor current increasing and decreasing periods. Device T_1 is turned on at t=0, at which the diode D_2 has reverse recovery loss. The switch on energy and power for T_1 can be calculated as follows:

$$\begin{aligned} E_{\text{on}} &= h_{\text{E,on},v} i^{k_{\text{E,on},v}}_{\text{L},v,\min} \\ P_{T_1,\text{on}} &= f_{\text{S},v} i^{k_{\text{P,on},v}}_{\text{L},v,\min} \end{aligned} \tag{36}$$

The reverse recovery energy and power for D_2 can be calculated as

$$\begin{aligned} E_{\text{Drr}} &= h_{\text{E,re},v} i^{k_{\text{E,re},v}}_{\text{L},v,\min} \\ P_{D2,\text{rr}} &= f_{\text{S},v} i^{k_{\text{P,re},v}}_{\text{L},v,\min} \end{aligned} \tag{37}$$

From $t = 0$ to $t = D_v T_S$, the current is flowing through T_1. The average current flowing through T_1 is $D_v i_{\text{L},v,\text{av}}$. The mean square current flowing through T_1 is $D_v(i^2_{\text{L},v,\text{av}} + \frac{\Delta i^2_{\text{L},v}}{12})$. Then the conduction loss for device T_1 is $V_{\text{T},v} D_v i_{\text{L},v,\text{av}} + D_v(i^2_{\text{L},v,\text{av}} + \frac{1}{12}\Delta i^2_{\text{L},v}) R_{\text{T},v}$.

From $t = D_v T_S$ to t=T_S, the current is flowing through D_2. The average current flowing through D_2 is $(1-D_v) i_{\text{L},v,\text{av}}$. The mean square current flowing through D_2 is $(1-D_v)(i^2_{\text{L},v,\text{av}} +$

[6] Δi_L is non-negative, as the $D_v \in [0, 1]$.

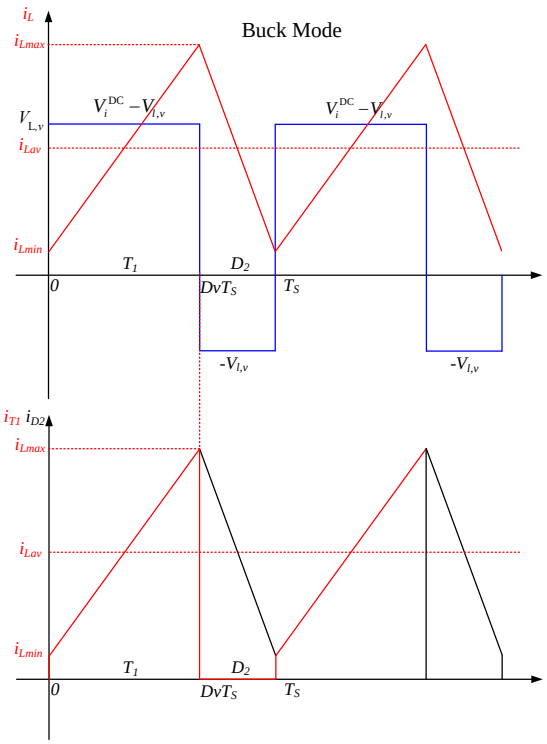

Fig. 12. Waveforms for power semiconductor losses calculation in buck mode.

$\frac{\Delta i_{\mathrm{L},v}^2}{12}$). The conduction loss for device D_2 is $V_{\mathrm{D},v}(1-D_v)i_{\mathrm{L},v,\mathrm{av}} + (1-D_v)(i_{\mathrm{L},v,\mathrm{av}}^2 + \frac{1}{12}\Delta i_{\mathrm{L},v}^2)R_{\mathrm{D},v}$.

The total loss for DC/DC converter in buck operation mode $p_{\mathrm{L},v}^{\mathrm{buck}}$ is shown in Eqn. (2).

The total loss in boost and buck-boost mode are given in Eqn. (3) and (4) respectively, which can be derived in a simialr way.

REFERENCES

[1] B. Chen, J. Wang, X. Lu, C. Chen, and S. Zhao, "Networked microgrids for grid resilience, robustness, and efficiency: a review," *IEEE Transactions on Smart Grid*, vol. 12, no. 1, pp. 18–32, 2020.

[2] Q. Xu, T. Zhao, Y. Xu, Z. Xu, P. Wang, and F. Blaabjerg, "A distributed and robust energy management system for networked hybrid ac/dc microgrids," *IEEE Transactions on Smart Grid*, vol. 11, no. 4, pp. 3496–3508, 2019.

[3] H. M. Ahmed and M. M. Salama, "Energy management of ac–dc hybrid distribution systems considering network reconfiguration," *IEEE Transactions on Power Systems*, vol. 34, no. 6, pp. 4583–4594, 2019.

[4] J.-S. Lai, L. Leslie, J. Ferrell, and T. Nergaard, "Characterization of hv-igbt for high-power inverter applications," in *Fourtieth IAS Annual Meeting. Conference Record of the 2005 Industry Applications Conference, 2005.*, vol. 1. IEEE, 2005, pp. 377–382.

[5] Q. Zhao, J. García-González, O. Gomis-Bellmunt, E. Prieto-Araujo, and F. Echavarren, "Impact of converter losses on the optimal power flow solution of hybrid networks based on vsc-mtdc," *Electric Power Systems Research*, vol. 151, pp. 395–403, 2017.

[6] H. Ergun, J. Dave, D. Van Hertem, and F. Geth, "Optimal power flow for ac–dc grids: Formulation, convex relaxation, linear approximation, and implementation," *IEEE Transactions on Power Systems*, vol. 34, no. 4, pp. 2980–2990, 2019.

[7] "IEEE standard for the specification of microgrid controllers," *IEEE Std 2030.7-2017*, pp. 1–43, 2018.

[8] X. Liu, P. Wang, and P. C. Loh, "A hybrid ac/dc microgrid and its coordination control," *IEEE Transactions on Smart Grid*, vol. 2, no. 2, pp. 278–286, 2011.

[9] W. Huang, W. Zheng, and D. J. Hill, "Distributionally robust optimal power flow in multi-microgrids with decomposition and guaranteed convergence," *IEEE Transactions on Smart Grid*, vol. 12, no. 1, pp. 43–55, 2021.

[10] M. N. Alam, S. Chakrabarti, and X. Liang, "A benchmark test system for networked microgrids," *IEEE Transactions on Industrial Informatics*, vol. 16, no. 10, pp. 6217–6230, 2020.

[11] B. Papari, C. S. Edrington, I. Bhattacharya, and G. Radman, "Effective energy management of hybrid ac–dc microgrids with storage devices," *IEEE transactions on smart grid*, vol. 10, no. 1, pp. 193–203, 2019.

[12] Z. Liang, H. Chen, X. Wang, S. Chen, and C. Zhang, "Risk-based uncertainty set optimization method for energy management of hybrid ac/dc microgrids with uncertain renewable generation," *IEEE Transactions on Smart Grid*, vol. 11, no. 2, pp. 1526–1542, 2019.

[13] B. Wei, X. Han, P. Wang, H. Yu, W. Li, and L. Guo, "Temporally coordinated energy management for ac/dc hybrid microgrid considering dynamic conversion efficiency of bidirectional ac/dc converter," *IEEE Access*, vol. 8, pp. 70 878–70 889, 2020.

[14] Y. Huang, Q. Sun, Y. Li, H. Zhang, and Z. Chen, "Adaptive-discretization based dynamic optimal energy flow for the heat-electricity integrated energy systems with hybrid ac/dc power sources," *IEEE Transactions on Automation Science and Engineering*, 2022.

[15] A. M. Shaheen, A. M. Elsayed, and R. A. El-Sehiemy, "Optimal economic–environmental operation for ac-mtdc grids by improved crow search algorithm," *IEEE Systems Journal*, vol. 16, no. 1, pp. 1270–1277, 2022.

[16] C. Nagaraj, "Reduction of power conversion losses in ac-dc coupled hybrid micro-grid under grid distorted voltage scenario," *Electric Power Systems Research*, vol. 210, p. 108101, 2022.

[17] J.-C. Fernández-Pérez, F. M. E. Cerezo, and L. R. Rodríguez, "Linear power flow algorithm with losses for multi-terminal vsc ac/dc power systems," *IEEE Transactions on Power Systems*, vol. 37, no. 3, pp. 1739–1749, 2022.

[18] Y. Fu, Z. Zhang, Z. Li, and Y. Mi, "Energy management for hybrid ac/dc distribution system with microgrid clusters using non-cooperative game theory and robust optimization," *IEEE Transactions on Smart Grid*, vol. 11, no. 2, pp. 1510–1525, 2020.

[19] Y. Zhang, X. Meng, A. M. Shotorbani, and L. Wang, "Minimization of ac-dc grid transmission loss and dc voltage deviation using adaptive droop control and improved ac-dc power flow algorithm," *IEEE Transactions on Power Systems*, vol. 36, no. 1, pp. 744–756, 2021.

[20] J. Ma, L. Yuan, Z. Zhao, and F. He, "Transmission loss optimization-based optimal power flow strategy by hierarchical control for dc microgrids," *IEEE Transactions on Power Electronics*, vol. 32, no. 3, pp. 1952–1963, 2016.

[21] H. Qiu, W. Gu, Y. Xu, and B. Zhao, "Multi-time-scale rolling optimal dispatch for ac/dc hybrid microgrids with day-ahead distributionally robust scheduling," *IEEE Transactions on Sustainable Energy*, vol. 10, no. 4, pp. 1653–1663, 2018.

[22] S. Bahrami, F. Therrien, V. W. Wong, and J. Jatskevich, "Semidefinite relaxation of optimal power flow for ac–dc grids," *IEEE Transactions on Power Systems*, vol. 32, no. 1, pp. 289–304, 2017.

[23] T. Wu, Y. J. Zhang, and X. Tang, "A vsc-based bess model for multi-objective opf using mixed integer socp," *IEEE Transactions on Power Systems*, vol. 34, no. 4, pp. 2541–2552, 2019.

[24] M. Isuru, M. Hotz, H. Gooi, and W. Utschick, "Network-constrained thermal unit commitment for hybrid ac/dc transmission grids under wind power uncertainty," *Applied Energy*, vol. 258, p. 114031, 2020.

[25] L. Zhao and B. Zeng, "An exact algorithm for two-stage robust optimization with mixed integer recourse problems," *submitted, available on Optimization-Online. org*, 2012.

[26] P. L. Querini, O. Chiotti, and E. Fernádez, "Cooperative energy management system for networked microgrids," *Sustainable Energy, Grids and Networks*, vol. 23, p. 100371, 2020.

[27] N. Nikmehr and S. N. Ravadanegh, "Optimal power dispatch of multi-microgrids at future smart distribution grids," *IEEE Transactions on Smart Grid*, vol. 6, no. 4, pp. 1648–1657, 2015.

[28] A. Mešanović, U. Muenz, and C. Ebenbauer, "Robust optimal power flow for mixed ac/dc transmission systems with volatile renewables," *IEEE Transactions on Power Systems*, vol. 33, no. 5, pp. 5171–5182, 2018.

[29] S. Teimourzadeh, O. B. Tor, M. E. Cebeci, A. Bara, and S. V. Oprea, "A three-stage approach for resilience-constrained scheduling of networked

microgrids," *Journal of Modern Power Systems and Clean Energy*, vol. 7, no. 4, pp. 705–715, 2019.
[30] B. Zhou, J. Zou, C. Y. Chung, H. Wang, N. Liu, N. Voropai, and D. Xu, "Multi-microgrid energy management systems: Architecture, communication, and scheduling strategies," *Journal of Modern Power Systems and Clean Energy*, vol. 9, no. 3, pp. 463–476, 2021.
[31] D. E. Olivares, J. D. Lara, C. A. Cañizares, and M. Kazerani, "Stochastic-predictive energy management system for isolated microgrids," *IEEE Transactions on Smart Grid*, vol. 6, no. 6, pp. 2681–2693, 2015.
[32] H. Qiu, W. Gu, Y. Xu, W. Yu, G. Pan, and P. Liu, "Tri-level mixed-integer optimization for two-stage microgrid dispatch with multi-uncertainties," *IEEE Transactions on Power Systems*, vol. 35, no. 5, pp. 3636–3647, 2020.
[33] X. Cao, X. Sun, Z. Xu, B. Zeng, and X. Guan, "Hydrogen-based networked microgrids planning through two-stage stochastic programming with mixed-integer conic recourse," *IEEE Transactions on Automation Science and Engineering*, pp. 1–14, 2021.
[34] J. Zou, S. Ahmed, X. A. Sun, and H. Stewart, "Nested decomposition of multistage stochastic integer programs with binary state variables," *Optimization Online*, vol. 5436, 2016.
[35] C. D'Ambrosio, A. Lodi, and S. Martello, "Piecewise linear approximation of functions of two variables in milp models," *Operations Research Letters*, vol. 38, no. 1, pp. 39–46, 2010.
[36] R. Henrion and W. Römisch, *Optimal scenario generation and reduction in stochastic programming*. Springer, 2018.
[37] L. Gan and S. H. Low, "Optimal power flow in direct current networks," *IEEE Transactions on Power Systems*, vol. 29, no. 6, pp. 2892–2904, 2014.
[38] R. Ahmed, V. Sreeram, Y. Mishra, and M. Arif, "A review and evaluation of the state-of-the-art in pv solar power forecasting: Techniques and optimization," *Renewable and Sustainable Energy Reviews*, vol. 124, p. 109792, 2020.
[39] T. Zhao, "Networked hybrid ac/dc microgrids with nonlinear conversion losses," 2022. [Online]. Available: https://dx.doi.org/10.21227/ayrv-ff02
[40] M. N. Alam, S. Chakrabarti, and A. Ghosh, "Networked microgrids: State-of-the-art and future perspectives," *IEEE Transactions on Industrial Informatics*, vol. 15, no. 3, pp. 1238–1250, 2019.

Tianyang Zhao (S'14-M'18-SM'22) received the B.Eng., M.Eng., and Ph.D. degrees in electrical engineering from North China Electric Power University, Beijing, China, in 2011, 2013, and 2017, respectively. He was a Postdoctoral Research Fellow with the Energy Research Institute, Nanyang Technological University, Singapore, from July 2017 to August 2020. Currently, he is an Associate Professor with Energy and Electricity Research Center, Jinan University. His research interests include operations research and resilience.

Xiong Liu (S'09–M'14–SM'19) received the B.E.and M.Sc. degrees in electrical engineering from Huazhong University of Science and Technology, Wuhan, China, in 2006 and 2008, respectively, and the Ph.D. degree from the School of Electrical and Electronic Engineering, Nanyang Technological University, Singapore in 2013.

From July to November 2008, he was an Engineer with Shenzhen Nanrui Technologies Company Ltd., Shenzhen, China. From September 2011 to January 2012, he was a Visiting Scholar with the Department of Energy Technology, Aalborg University, Aalborg East, Denmark. From April 2012 to December 2013, he was a Researcher with the Energy Research Institute, Nanyang Technological University. From December 2013 to July 2020, He was working as a Principal Technologist in Rolls-Royce Electrical, Rolls-Royce Singapore Pte. Ltd., Singapore. He is currently an Associate Professor with the Energy Electricity Research Center, International Energy College, Jinan University, Zhuhai, China. His research interests include power electronics, motor drive, and electrical/hybrid propulsion system for marine and aerospace.

Dr. Liu was the recipient of the Best Paper Award at the IEEE International Power Electronics and Motion Control Conference-Energy Conversion Congress and Exposition Asia in 2012

Peng Wang (F'18) received the B.Sc. degree in electronic engineering from Xian Jiaotong University, Xian, China, in 1978, the M.Sc. degree from Taiyuan University of Technology, Taiyuan, China, in 1987, and the M.Sc. and Ph.D. degrees in electrical engineering from the University of Saskatchewan, Saskatoon, SK, Canada, in 1995 and 1998, respectively. Currently, he is a Professor with the School of Electrical and Electronic Engineering at Nanyang Technological University, Singapore.

Frede Blaabjerg (S'86–M'88–SM'97–F'03) was with ABB-Scandia, Randers, Denmark, from 1987 to 1988. From 1988 to 1992, he got the PhD degree in Electrical Engineering at Aalborg University in 1995. He became an Assistant Professor in 1992, an Associate Professor in 1996, and a Full Professor of power electronics and drives in 1998 at AAU Energy. From 2017 he became a Villum Investigator. He is honoris causa at University Politehnica Timisoara (UPT), Romania in 2017 and Tallinn Technical University (TTU), Estonia in 2018.

His current research interests include power electronics and its applications such as in wind turbines, PV systems, reliability, harmonics and adjustable speed drives. He has published more than 600 journal papers in the fields of power electronics and its applications. He is the co-author of four monographs and editor of ten books in power electronics and its applications.

He has received 38 IEEE Prize Paper Awards, the IEEE PELS Distinguished Service Award in 2009, the EPE-PEMC Council Award in 2010, the IEEE William E. Newell Power Electronics Award 2014, the Villum Kann Rasmussen Research Award 2014, the Global Energy Prize in 2019 and the 2020 IEEE Edison Medal. He was the Editor-in-Chief of the IEEE TRANSACTIONS ON POWER ELECTRONICS from 2006 to 2012. He has been Distinguished Lecturer for the IEEE Power Electronics Society from 2005 to 2007 and for the IEEE Industry Applications Society from 2010 to 2011 as well as 2017 to 2018. In 2019-2020 he served as a President of IEEE Power Electronics Society. He has been Vice-President of the Danish Academy of Technical Sciences. He is nominated in 2014-2021 by Thomson Reuters to be between the most 250 cited researchers in Engineering in the world.